*Bangladesh Journal of Physics, Vol. **32**, Issue 2, pp. 43 – 52, December 2025*

THERMAL ANNEALING-INDUCED ENHANCEMENT OF CRYSTALLINITY AND OPTICAL RESPONSE IN SPIN-COATED Cu_2FeSnS_4 THIN-FILM ABSORBERS

M. M. RASHID[1*], S. AKHTER[1], S. BHATTACHARJEE[1], M. S. BASHAR[2], AND S. J. AHMED[1]

[1]*Department of Physics, Dhaka University of Engineering & Technology, Gazipur, Bangladesh*
[2]*Institute of Fuel and Research Development, BCSIR, Bangladesh*

[*]*Corresponding author email: mamun92@duet.ac.bd, jasyed111@duet.ac.bd*
Received on 20.11.2025, Revised received on 29.12.2025, Accepted for publication on 31.12.2025

DOI: ***https://doi.org/10.3329/bjphy.v32i2.85736***

ABSTRACT

This study investigates the effect of annealing temperature (AT) on the structural and optical properties of CFTS (Cu_2FeSnS_4) thin films fabricated via the spin coating technique on glass substrates. The films were annealed at 300 °C, 340 °C, and 380 °C. X-ray diffraction confirms that all films crystallize in the stannite structure, with higher AT enhancing crystallinity, increasing crystallite size, and reducing lattice defects. Optical characterization reveals that absorbance, absorption coefficient ($\sim 10^4$ cm^{-1}), and refractive index increase with AT, while the optical band gap shows a decreasing trend. Optical conductivity also rises, indicating improved charge carrier mobility and electronic response. These findings demonstrate that optimized annealing enhances the structural and optical quality of CFTS films, confirming their potential as efficient absorber layers for thin-film solar cells.

Key-words: *CFTS thin films, annealing temperature, structural properties, optical properties*

1. INTRODUCTION

The rapid growth in global energy demand underscores the urgent need for sustainable and renewable energy solutions. Among the available options, solar energy is particularly attractive due to its abundance, environmental friendliness, and long-term sustainability. Recent advances in thin-film photovoltaic technologies have significantly improved device efficiency while reducing production costs, owing to their low material consumption, lightweight nature, and suitability for large-area fabrication [1]. Copper-based quaternary chalcogenides of the I_2-II-IV-VI_4 family, including Cu_2ZnSnS_4 (CZTS) [2,3], $Cu_2ZnSnSe_4$ (CZTSe) [4], Cu_2NiSnS_4 (CNTS) [5-7], and Cu_2FeSnS_4 (CFTS) [5,8-16], have attracted considerable attention as absorber materials for thin-film solar cells. These compounds possess crystal structures similar to $Cu(In,Ga)(S,Se)_2$ (CIGS) while being composed of earth-abundant and non-toxic elements, making them promising candidates for low-cost and large-scale photovoltaic applications [2-16]. Among them, CZTS has been the most extensively investigated and has achieved a power conversion efficiency of 13.2 % [17].

Recently, CFTS has emerged as a promising alternative absorber material due to its favorable optoelectronic properties and the use of abundant, low-cost elements such as Fe and Sn. CFTS exhibits a suitable optical bandgap of approximately 1.5 eV and a high absorption coefficient on the order of 10^4-10^5 cm^{-1}, making it an excellent candidate for efficient light absorption and energy conversion in thin-film photovoltaic devices [5,8-16,18-22]. Beyond photovoltaic absorbers, CFTS thin films have also demonstrated potential in other solar-energy applications. For instance, dye-

sensitized solar cells employing CFTS as a counter electrode have achieved a power conversion efficiency of 8.03 %, indicating that CFTS is a cost-effective alternative to Platinum [23]. CFTS thin films have been synthesized using various techniques, including thermal evaporation [6], electrochemical deposition [8], spin coating [11], spray pyrolysis [16], vacuum evaporation [24], sputtering [25-27], liquid reflux [28], ultrasound-assisted microwave [29], hot injection [30], and solvothermal methods [31].

Despite these advances, a systematic understanding of the influence of post-deposition annealing temperature on the structural and optical properties of spin-coated CFTS thin films remains limited. In particular, the correlation between annealing-induced crystallinity improvement, defect reduction, and optical properties evolution has not been sufficiently clarified. In this work, we systematically investigate the structural and optical evolution of spin-coated CFTS thin films annealed over a controlled temperature range. The present study establishes a clear relationship between annealing temperature and material quality, providing insight into defect reduction and band-gap tuning mechanisms.

2. EXPERIMENTAL DETAILS

In this study, Cu_2FeSnS_4 (CFTS) thin films were fabricated on glass substrates using a spin coating technique. $CuCl_2 \cdot 2H_2O$, $FeCl_3 \cdot 6H_2O$, $SnCl_2 \cdot 2H_2O$, and $SC(NH_2)_2$—serving as the sources of Cu, Fe, Sn, and S, respectively—were dissolved in 2-methoxyethanol, a high-boiling-point organic solvent that ensures uniform dissolution and prevents premature evaporation. A few drops of mono-ethanolamine were then added as a stabilizing agent to promote smooth and homogeneous film formation. The solution was stirred at 50 °C for 60 minutes using a magnetic stirrer (Model: 78-1 Magnetic Heating Stirrer, China) to achieve a fully homogeneous brown-coloured precursor solution. The prepared solution was deposited onto glass substrates using a vacuum spin coater (Model: VTC-100PA, Germany) at 2000 rpm for 1 minute. After each coating, the substrates were preheated at 120 °C for 10 minutes to remove residual solvent and partially densify the film. To achieve the desired film thickness, the spin coating and preheating cycle were repeated eight times. Following deposition, the films underwent post-annealing in a furnace (Model: KLS10/12, Germany) at 300 °C, 340 °C, and 380 °C for 30 minutes to induce re-crystallization and improve structural quality. The annealed samples were designated as S1-T300, S2-T340, and S3-T380 corresponding to annealing temperatures of 300 °C, 340 °C, and 380 °C, respectively. The structural properties of the deposited CFTS thin films were examined using X-ray diffraction (Model: BRUKER D8 XRD, Germany), and their optical properties were characterized using UV—visible spectroscopy (Model: UH4150 spectrophotometer, Japan).

3. RESULTS AND DISCUSSION

3.1 Structural Analysis

The X-ray diffraction (XRD) patterns of the CFTS (Cu_2FeSnS_4) thin films annealed at 300 °C (S1-T300), 340 °C (S2-T340), and 380 °C (S3-T380) are presented in Fig. 1. The as-deposited CFTS thin film usually exhibited an amorphous or poorly crystalline nature due to insufficient thermal energy during deposition, resulting in the absence of well-defined diffraction peaks associated with long-range structural ordering. Therefore, the XRD pattern of the as-deposited film is not shown,

and the discussion focuses on the structural evolution induced by post-deposition annealing. All annealed samples exhibit four prominent diffraction peaks corresponding to the (112), (200), (220), and (312) crystallographic planes. These reflections can be indexed to the tetragonal stannite structure of CFTS (space group *I*-42*m*), and their positions match well with the standard reference data from the JCPDS card No. 44-1476 [31,32], confirming the successful formation of the CFTS phase. Furthermore, the peak positions remain unchanged with increasing annealing temperature (AT), suggesting that the crystal structure of CFTS is preserved throughout the annealing process. Among the observed reflections, the (112) peak exhibits the highest intensity for all ATs, indicating a preferred orientation along this crystallographic direction, which is a commonly reported feature of kesterite- and stannite-based quaternary chalcogenide absorber layers. The crystallinity of the films is strongly influenced by the AT. At 300 °C, the diffraction peaks are relatively broad and weak, implying small crystallite size, internal strain, and a high density of lattice defects due to limited atomic diffusion. With increasing AT to 340 °C and 380 °C, the diffraction peaks become progressively sharper and more intense, reflecting enhanced crystallite growth, reduced microstrain, and improved long-range structural ordering. This improvement in crystallinity can be attributed to a thermally activated grain-growth mechanism, where increased thermal energy enables atoms to overcome kinetic barriers, migrate to energetically favorable lattice sites, and reduce lattice imperfections [33].

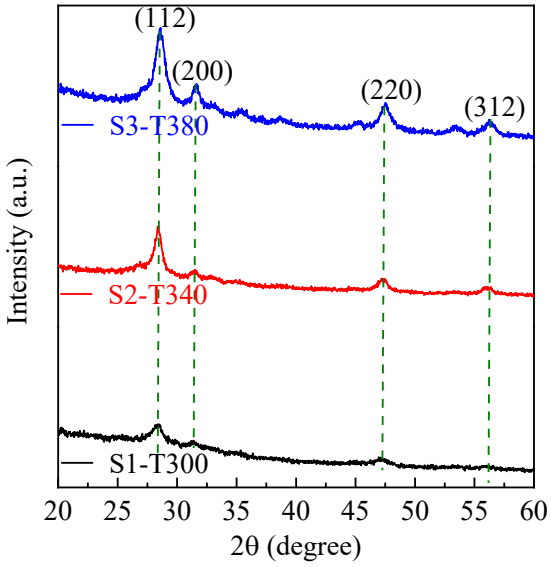

Fig. 1 XRD patterns of CFTS thin films annealed at 300 °C, 340 °C, and 380 °C.

To further quantify these effects, the microstructural parameters i.e., crystallite size (D), microstrain (ε), and dislocation density (δ) were calculated using the prominent (112) peak using the following Scherrer relations [7,24]:

$$D = \frac{K_S\lambda}{\beta Cos\theta} \text{.....(1)}$$

$$\varepsilon = \frac{\beta\, Cos\theta}{4} \text{.....(2)}$$

$$\delta = \frac{1}{D^2} \text{.....(3)}$$

Here, λ is the X-ray wavelength (0.15406 nm), K_S is the Scherrer constant (0.9), β is the full width at half maximum in radians and θ is the Bragg angle in radians.

Figure 2 shows the variation of crystallite size, microstrain, and dislocation density of CFTS thin films as a function of AT. The increase in crystallite size and simultaneous decrease in microstrain and dislocation density correlate with the XRD observations: sharper and more intense diffraction peaks at higher temperature indicates enhanced grain growth, reduced lattice strain, and fewer defects. These results confirm that thermally activated atomic diffusion during annealing promotes coalescence of smaller crystallites and defect annihilation, improving long-range structural ordering. The trends highlight the critical role of optimizing AT to obtain high-quality, well-crystallized CFTS thin films suitable as absorber layers in photovoltaic applications, consistent with prior reports on CFTS and related quaternary chalcogenides [24,34,35].

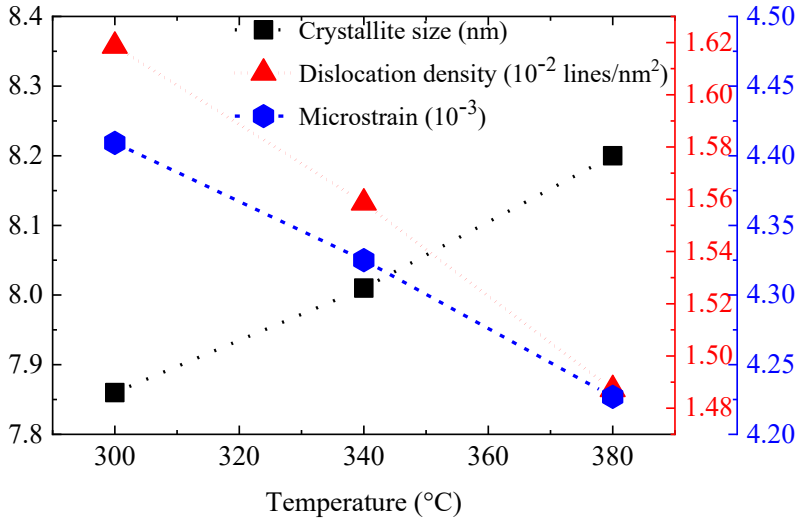

Fig. 2 Variation of crystallite size, microstrain and dislocation density of CFTS thin films as a function of AT.

3.2 Optical Analysis

Figure 3 presents the absorbance spectra of S1-T300, S2-T340, and S3-T380 thin films as a function of wavelength. An increase in absorbance is observed with higher AT, which can be attributed to improved crystallinity at elevated AT. Enhanced crystallinity reduces structural defects and increases the optical density of the films, allowing more efficient light absorption. Additionally, the overall decrease in absorbance with increasing wavelength is consistent with the fundamental principle that lower-energy photons (longer wavelengths) are less effective at promoting electrons across the bandgap, resulting in reduced absorption [36].

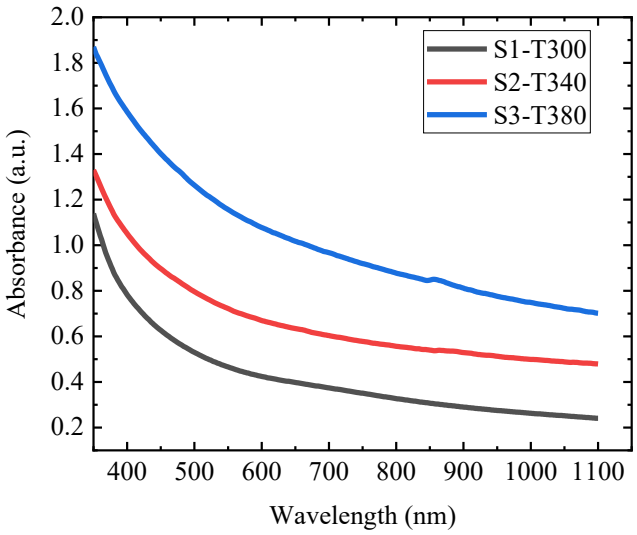

Fig.3 Absorbance (*A*) spectra of the deposited CFTS thin films as a function of wavelength.

The absorption coefficient (α) of CFTS thin films was calculated using the following relation [7] and illustrated in Fig. 4:

$$\propto = \frac{2.303\ A}{t} \quad \text{.....(4)}$$

where t is the thickness of the film, approximately 500 nm.

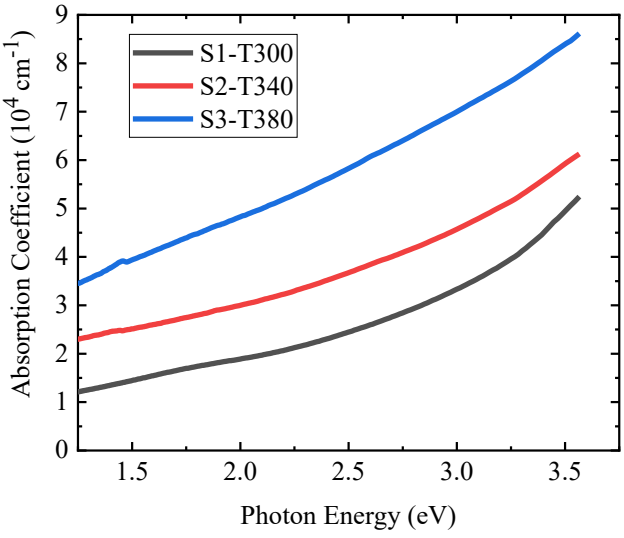

Fig. 4 Absorption coefficient of the deposited CFTS thin films as a function of photon energy.

Figure 4 illustrates the variation of the absorption coefficient with photon energy, providing detailed insights into the band structure and the nature of electronic transitions responsible for light absorption. The absorption coefficient is found to increase with the increase of AT. Additionally, it increases sharply with increasing photon energy, and the pronounced rise in the higher photon energy range indicates that direct electronic transitions dominate the absorption process in these films. The absorption coefficient is found to be on the order of $\sim 10^4$ cm^{-1}, which is consistent with previously reported values for similar CFTS thin films [37,38]. Since CFTS thin films are intended for use as absorber layers in solar cells, a high absorption coefficient is essential to ensure efficient photon capture. Therefore, these results demonstrate that the fabricated CFTS thin films exhibit strong light-harvesting capabilities and are well-suited for use as absorber layers in photovoltaic devices, highlighting their potential for high-performance solar energy conversion [38-40].

Building upon the previously discussed absorbance and absorption-coefficient analyses, the optical band gap (E_g) of CFTS thin films were determined using the following Tauc relation, which is widely used to evaluate the optical band gap of semiconductor thin films by relating the absorption coefficient to the photon energy [7,24].

$$\alpha h\nu = A_0(h\nu - E_g)^n \quad \text{.....(5)}$$

Here A_0 is the energy dependent constant and n is the refractive index.

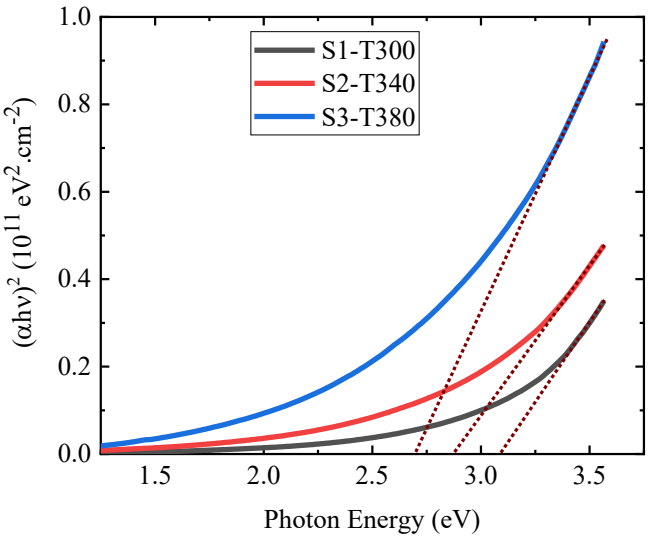

Fig. 5 $(\alpha h\nu)^2$ versus photon energy $(h\nu)$ curves of different CFTS thin films.

Figure 5 shows the $(\alpha h\nu)^2$ versus $h\nu$ plots for S1-T300, S2-T340, and S3-T380 thin films. The linear portions of these plots were extrapolated to the energy axis ($(\alpha h\nu)^2 = 0$) to determine the optical band gap values. A clear decrease in the optical band gap is observed with AT, from 3.09 eV for S1-T300 to 2.69 eV for S1-T380. The reduction in band gap with increasing AT is primarily attributed to improvements in crystallinity and a reduction in structural disorder with AT. As annealing promotes grain growth and reduces disorder, localized defect states are minimized, resulting in a narrowing of the optical band gap toward the value characteristic of well-crystalline material. Although the band gap decreases with AT, the obtained values remain significantly higher

than the ideal bulk band gap of CFTS (~1.5 eV). These comparatively large band gap values represent apparent optical band gaps influenced by structural disorder, defect-related localized states, and limited long-range ordering, particularly in films annealed at lower temperatures. These findings suggest that further or optimized annealing may shift the band gap of CFTS films closer to the intrinsic values reported in the literature, indicating potential for further improvement in optical properties.

The refractive index (n) of CFTS thin films was calculated using the following relation [7] and illustrated in Fig. 6:

$$n = \frac{1+R}{1-R} + \sqrt{\frac{4R}{(1-R)^2} - {k_E}^2} \quad \text{.....(6)}$$

Here R and k_E represent the reflectance and extinction coefficient, respectively.

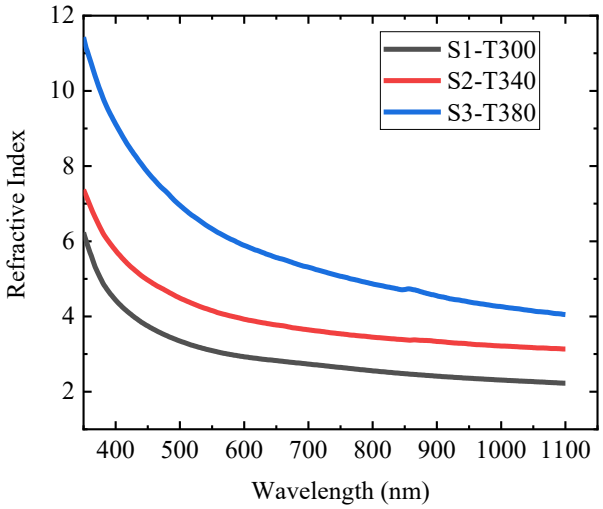

Fig. 6 Refractive of the deposited CFTS thin films as a function of wavelength.

Figure 6 presents the refractive index of the S1-T300, S2-T340, and S3-T380 CFTS thin films as a function of wavelength. Consistent with the earlier optical results, the refractive index increases systematically with increasing AT. The S3-T380 film exhibits the highest refractive index across the entire wavelength range, followed by S2-T340 and S1-T300. This trend correlates strongly with the improvements in crystallinity, reduction of lattice defects, and the increase in film density observed in earlier analyses. As demonstrated from the absorbance and absorption-coefficient results, higher ATs promote enhanced light-matter interaction due to improved structural ordering and fewer scattering centers. Additionally, the observed increase in refractive index aligns with the previously noted decrease in optical band gap. According to the Moss relation ($n^4 E_g = \text{constant}$) [41], the band-gap narrowing in the high-temperature films (from 3.09 eV to 2.69 eV) naturally leads to an increase in refractive index. The decreasing trend of n with wavelength for all samples also reflects typical normal dispersion behavior in semiconductor thin films.

The optical conductivity (σ_{opt}) of the fabricated CFTS thin films is determined using the following equation [7] and illustrated in Fig. 7,

$$\sigma_{opt} = \frac{\alpha nc}{4\pi} \text{ .....(7)}$$

Here c is the speed of light speed.

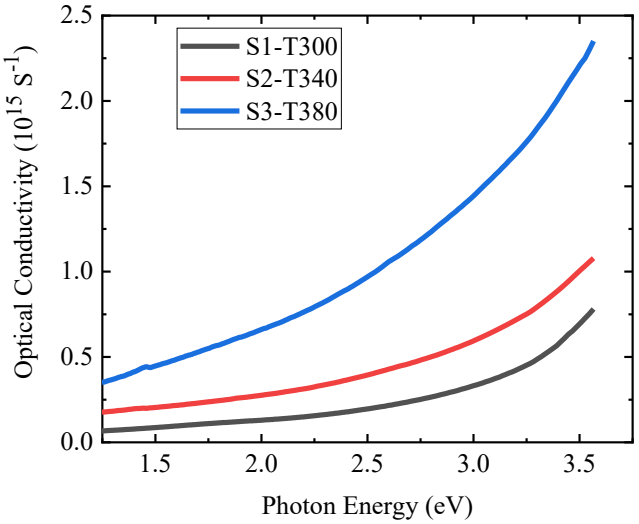

Fig. 7 Optical conductivity of the deposited CFTS thin films as a function of photon energy.

Figure 7 shows the variation of optical conductivity as a function of photon energy for CFTS thin films annealed at different temperatures. The optical conductivity increases consistently with rising AT. This behavior can be attributed to the concurrent enhancement of the absorption coefficient and refractive index, along with the reduction in %T at higher AT. As annealing improves crystallinity, minimizes defect states, and enhances the overall optical density of the films, a large number of incident photons are effectively absorbed, generating more photo-excited charge carriers. Since σ_{opt} is directly related to the mobility and density of these photo-generated carriers, improved structural and optical quality naturally leads to higher σ_{opt}. Additionally, σ_{opt} increases steadily with photon energy. This is expected, as higher-energy photons can excite electrons more efficiently, thereby increasing the number and activity of photo-generated carriers within the film [42]. The enhanced motion of these carriers at elevated photon energies further strengthens the optical conductivity response. Therefore, the increasing trend of σ_{opt} with AT confirms that AT plays a significant role in tuning the photo-response behavior of CFTS thin films by promoting better carrier generation and transport.

In this study, we found that the combined structural and optical results confirm that annealing temperature strongly governs the quality of CFTS thin films. Higher annealing enhances crystallinity, enlarges crystallite size, and reduces defects, leading to improved structural order. These improvements directly enhance optical properties, including higher absorption, refractive index, and optical conductivity, along with a slight reduction in band gap due to fewer defect states. Overall, proper annealing significantly boosts the optoelectronic performance of CFTS thin films, making them more suitable for photovoltaic applications.

4. CONCLUSIONS

In summary, this study demonstrates that annealing temperature (AT) significantly influences the structural and optical properties of CFTS (Cu_2FeSnS_4) thin films. XRD analysis confirmed that all films crystallize in the stannite structure and revealed that increasing the AT from 300 °C to 380 °C enhances crystallinity, promotes grain growth, and reduces lattice defects, leading to improved structural ordering and film density. These structural improvements directly affect the optical properties: both absorbance and the absorption coefficient increase with AT, with the highest-temperature film (S3-T380) exhibiting an absorption coefficient on the order of $\sim 10^4$ cm^{-1}, indicating strong light-harvesting potential suitable for photovoltaic applications. The refractive index also rises with AT, reflecting increased optical density and fewer scattering centers. Simultaneously, the optical band gap decreases from 3.09 eV to 2.69 eV, consistent with improved atomic ordering and reduced defect states in the lattice. The optical conductivity increases with AT, indicating enhanced charge carrier mobility and improved electronic response. These results show that optimizing annealing conditions strengthens the stannite structure and enhances light absorption and electronic transport. Overall, this improves the optical and structural quality of CFTS thin films, highlighting their potential as efficient absorber layers for thin-film solar cells.

ACKNOWLEDGEMENTS

The authors gratefully acknowledge the financial & technical support provided by Dhaka University of Engineering & Technology, Gazipur, Bangladesh.

REFERENCES

[1] M. A. Green, E. D. Dunlop, J. Hohl-Ebinger, M. Yoshita, N. Kopidakis, and A. W. Y. Ho-Baillie, Prog. Photovolt.: Res. Appl. **28** (2020) 3.

[2] F. Z. Boutebakh, N. Attaf, and M. S. Aida, Discover Mater. **5** (2025) 4.

[3] Z. Kişnişci, F. Özel, N. Tuğluoğlu, and Ö. F. Yüksel, Opt. Quantum Electron. **56** (2024) 1239.

[4] Ö. Demircioğlu, J. F. L. Salas, G. Rey, T. Weiss, M. Mousel, A. Redinger, S. Siebentritt, J. Parisi, and L. Gütayet, Opt. Express **25** (2017) 5327.

[5] A. Ghosh, A. Biswas, R. Thangavel, and G. Udayabhanu, RSC Adv. **6** (2016) 96025.

[6] I. Abdelaziz, E. Gnenna, D. Khelifi, M. ben Rabeh, and M. Kanzari, IEEE (2024 IEEE Int. Conf. Artif. Intell. Green Energy (Tunisia) pp-1 (2024).

[7] M. M. Rashid, A. A. Noman, S. Islam, F. Ahmed, M. S. Bashar, M. S. Uddin, A. T. M. K. Jamil, S. J. Ahmed, Bangladesh J. Phys. **28** (2021) 39.

[8] X. Miao, R. Chen, and W. Cheng, Mater. Lett. **193** (2017) 183.

[9] S. A. Vanalakar, P. S. Patil, and J. H. Kim, Sol. Energy Mater. Sol. Cells **182** (2018) 204.

[10] F. K. Konan, H. T. Nkuissi, and B. Hartiti, Int. J. Renew. Energy Res. **9** (2019) 9816.

[11] S. Islam, P. Majumdar, M. A. Hossain, and F. Ahmed, J. Mater. Sci. Eng. A **12** (2022) 5.

[12] R. Deepika and P. Meena, Mater. Res. Express **7** (2020) 035012.

[13] V. Trifiletti, G. Tseberlidis, M. Colombo, A. Spinardi, S. Luong, M. Danilson, M. Grossberg, O. Fenwick, and S. Binetti, Mater. **13** (2020) 1471.

[14] S. P. Madhusudanan, M. Suresh Kumar, K. Mohanta, and S. K. Batabyal, Appl. Surf. Sci. **535** (2021) 147600.

[15] E. Waluś, M. Manecki, and G. Cios, Mater. **13** (2020) 4440.

[16] C. Nefzi, M. Souli, B. Jeyadevan, and N. Kamoun-Turki, J. Phys. Chem. Solids **144** (2020) 109497.

[17] https://solarbytes.info/tech-bytes/unsw-world-record-kesterite-czts-solar-efficiency-8660703

[18] X. Zhang, N. Bao, K. Ramasamy, Y.-H.A. Wang, Y. Wang, B. Lin, A. Gupta, Chem. Commun. **48** (2012) 4956.

[19] C. Yan, C. Huang, J. Yang, F. Liu, J. Liu, Y. Lai, J. Li, Y. Liu, Chem.Commun. **48** (2012) 2603.

[20] F. Liu, Y. Li, K. Zhang, B. Wang, C. Yan, Y. Lai, Z. Zhang, J. Li, Y. Liu, Sol. Energ. Mater. Sol. Cells **94** (2010) 2431.

[21] C. Domain, S. Laribi, S. Taunier, J.F. Guillemoles, J. Phys. Chem. Solids **64** (2003) 1657.

[22] X. Song, X. Ji, M. Li, W. Lin, X. Luo, H. Zhang, Inter. J. Photoenergy **2014** (2014) 1.

[23] R.R. Prabhakar, N.H. Loc, M.H. Kumar, P.P. Boix, S. Juan, R.A. John, S.K. Batabyal, L.H. Wong, ACS Appl. Mater. Interfaces **6** (2014) 17661.

[24] H. Oueslati, M. ben Rabeh, and M. Kanzari, Appl. Phys. A **124** (2018) 201.

[25] H. X.Meng, L. Deng, P. Sun, Yang, J. Chu, Mater. Lett. **161** (2015) 427.

[26] X. Meng, H. Deng, J. Tao, H. Cao, X. Li, L. Sun, P. Yang, J. Chu, J. Alloys Compd. **680** (2016) 446

[27] X. Meng, H. Deng, Q. Zhang, L. Sun, P. Yang, J. Chu, Mater. Lett. **186** (2017) 138

[28] J. Zhou, Z. Ye, Y. Wang, Q. Yi, J. Wen, Mater. Lett. **140** (2015) 119

[29] W. Wang, H. Shen, H. Yao, J. Li, Mater. Lett. **125** (2014) 183

[30] Y. Liu, M. Hao, J. Yang, L. Jiang, C. Yan, C. Huang, D. Tang, F. Liu, Y. Liu, Mater. Lett. **136** (2014) 306

[31] X. Jiang, W. Xu, R. Tan, W. Song, J. Chen, Mater. Lett. **39** (2013) 102

[32] H. Guan, H. Shen, B. Jiao, and X. Wang, Materials Science in Semiconductor Processing **25** (2014) 159.

[33] H. Katagiri, K. Jimbo, W. S. Maw, K. Oishi, M. Yamazaki, H. Araki, and A. Takeuchiet, Thin Solid Films **517** (2009) 2455.

[34] A. A. Ahmad, A. B. Migdadi, A. M. Alsaad, I. A. Qattan, Q. M. Al-Bataineh, and A. Telfah, Heliyon **8** (2022) e08683.

[35] O. E. Khouja, C. C. Negrila, K. Nouneh, M. Secu, M. E. Touhami, E. Matei, V. Stancu, M. Enculescu, V. Kuncser, and A. C. Galca, J. Alloys Compd. **906** (2022) 164379.

[36] D. Kumar, A. Singh, N. Kaur, A. Katoch, and R. Kaur, Korean J. Mater. Res. **32** (2022) 249.

[37] H. I. el Saeedy, H. A. Yakout, and M. T. el Sayed, Appl. Phys. A 126 (2020) 281.

[38] C. Dong, G. Y. Ashebir, J. Qi, J. Chen, Z. Wan, W. Chen, and M. Wang, Mater. Lett. **214** (2018) 287.

[39] M. A. Abed, N. A. Bakr, and S. B. Mohammed, Mater. Sci. Forum **1039** (2021) 434.

[40] A. le Donne, V. Trifiletti, and S. Binetti, Front. Chem. **7** (2019) 297.

[41] A. Lamichhane, Solids **4** (2023) 316.

[42] R. Nasrin, H. Kabir, H. Akter, and A. H. Bhuiyan, Results Phys. **19** (2020) 103357.